Journal of Materials Chemistry C

ROYAL SOCIETY OF CHEMISTRY

PAPER

View Article Online
View Journal

Cite this: DOI: 10.1039/d2tc03254f

An optimal climate-adaptable hydrogel-filled smart window for the energy-saving built environment†

Anurag Roy, * Tapas K. Mallick and Asif Ali Tahir *

Received 2nd August 2022,
Accepted 18th September 2022

DOI: 10.1039/d2tc03254f

rsc.li/materials-c

It is highly desirable to secure the net-zero targets by employing sustainable building materials that can store and release their energy depending on the weather. Conspicuously, windows can play a pivotal role in controlling the energy used in the building by reducing the use of energy-consuming areas that devour massive energy for air conditioning or heating appliances. Presently, the comfort performance of window materials is reaching its storage and processing limit, causing a significant push to find smart materials that can be used in the next generation of the built environment. An innovative solution for sustainable glazing has established an understanding of pH-temperature-transparency modulation. This work uses a hydroxypropyl cellulose and polyacrylic acid-based hydrogel as a rational energy stimulus for double-glazed windows, enriching a comfortable indoor daylight environment without sacrificing aesthetic appeal. The hydrogel maintains thermal comfort across various outdoor temperatures from 4 °C to 60 °C. The developed hydrogel-filled prototype glazing's indoor thermal comfort performance and durability were analsyzed, where the hydrogel intermolecular gap and porosity play a pivotal role across various pHs.

Introduction

Every technology in our society will be needed in the battle to bring climate change under control. Including renewable energy, the net-zero emission target can also be achieved by some other alternative routes, especially with the built environment. This is because there has been a phenomenal growth in buildings and construction industries, which have to secure net-zero targets by employing sustainable materials that can store and release their energy through solar technology to retrofit existing non-smart windows. This further implies deriving an energy-positive built environment.[1] National/local decision-makers should adopt thermal and local urban planning regulations to include minimum glazed surfaces in new constructions and significant renovations.[2] Applying solar technology to retrofit existing traditional, humdrum windows is one of the potential sectors for energy-positive built environments. Smart windows could create an energy-positive built environment through their heat loss or gain strategy, depending on the climate. Hence, the exotic behaviour of the chemical system enabling thermal comfort of the house through a window has long been an emerging topic of interest.

Dominantly the near-infrared (NIR) wavelengths are responsible for the house's high energy absorption and thermal discomfort during different seasons. Therefore, NIR reflecting windows could be a suitable option that takes a leading step to achieving energy-positive buildings.[3–5] A significant proportion (>30%) of heat is released or gained through the window, which controls the building thermal comfort level, where the window glass coating or glazing materials offer real benefits and assist ongoing international carbon emission targets with minimum energy guzzling.[6] Development/identification of less expensive transparent insulating materials for windows is the solution to cut down electricity charges for modern thermal comfort providers and daylighting systems in buildings. Recently, cost-effective and easy-to-prepare thermochromic-heat storage hydrogels have been unrolled as suitable alternative materials among traditional window glazing options.

The benefits of using hydrogels are cost-effectiveness, environment-friendly nature, biocompatibility, thermo-responsive liquid-trapped structures, easy fabrication, good uniformity, and scalability. Nevertheless, hydrogels are stimulus-sensitive, depending on the matrix temperature, pH, ionic strength, *etc.*[7] Hydrogels form networks of hydrophilic polymer chains with an aqueous-rich environment, which have already been dominantly used in multiple areas. Hydrogels can exhibit reversible hydrophilic/hydrophobic phase transitions around the lower critical

Environment and Sustainability Institute, Faculty of Environment, Science and Economy, University of Exeter, Penryn Campus, Cornwall TR10 9FE, UK.
E-mail: a.roy30@exeter.ac.uk, a.tahir@exeter.ac.uk

† Electronic supplementary information (ESI) available: Video of HPC–PAA hybrid hydrogel window, working under 1 sun light condition during its ON and OFF time exhibits a distinct change of transparency from transparent to translucent for a warmer climate. See DOI: **https://doi.org/10.1039/d2tc03254f**

solution temperature (LCST).[8–10] Simultaneous thermochromism and cool/warm tone switchability functions of hydrogels can be beneficial for smart windows.

Smart windows *via* sandwiching a poly(*N*-isopropylacrylamide) (PNIPAm) hydrogel were proposed by Long *et al.* (2014).[11] Tuning the hydrogel thickness can change the thermochromic optical transmission spectra and hence the incoming heat. Hydroxypropyl cellulose (HPC) as a water-soluble cellulose derivative was found to be a LCST hydrogel where the temperature was reduced from 42 to 30 °C, controlling the transmissivity and reflectivity of the glazing unit.[12] Cheng *et al.* (2018) reported reversible color/transparency switching characteristics with an Au nanocrystal incorporated hydroxypropyl methylcellulose (HPMC) hydrogel.[13] The thermochromic hydrogels regulate light transmission *via* electrical heating as well. Recently, HPC with a polyacrylic acid (PAA)-based hydrogel exhibited outstanding heat-shielding performance as recorded for up to 100 heating and cooling cycles with a comfortable room temperature range (*e.g.*, 26–28 °C) for warmer climates.[14]

N-Vinylcaprolactam (PNVCL) was found to be an active material in the smart window owing to their morphological changes over time. Long *et al.* (2020) developed a revolutionary high-energy, thermo-responsive smart window that can cut off 44.6% heating with soundproof functionality by trapping the hydrogel.[15] Besides, the reversible and dynamic nature of the electrostatic and hydrogen bonds of the poly(acrylic acid) (PAA) structure makes it a potential component for hydrogel formation.[16–18] HPC exhibits a high LCST of 42 °C, hindering its practical smart window applications.[19,20] However, supplementary hydrogen bonding with hydrophobic polymers such as PAA can reduce the LCST of HPC by forming a stable temperature-responsive complex.[21–23]

This work reveals a HPC–PAA-based temperature-responsive hydrogel that could possess a heat-shielding effect with suitable lower critical solution temperature across a wide range of pH (3.5–5.5). Intermolecular hydrogen bonds that prevail between the polymer chains and surrounding water molecules with the porous structure of HPC–PAA, offer heat-shielding and further visible transparency by varying the pH and temperature of the gel. The developed smart windows exhibit an average temperature of ∼28 °C once the outdoor temperature reaches ∼45 °C, whereas at colder temperatures (∼4 °C), the same window furnishes an indoor temperature of ∼18 °C. This work also signifies a cost-effective, biocompatible alternative solution to traditional vacuum-based, polydispersed liquid, inert-gas-filled windows for use in the smart window technology and promises no energy consumption during operation without sacrificing aesthetic appeal. Notably, this study also focuses on the opto-thermal performance of hydrogel-filled windows at lower temperatures (<20 °C), which is quite limited to be analyzed.

Materials and methods

Synthesis of hybrid HPC/PAA hydrogels

The hybrid hydrogel was made by a similar process reported by Gao *et al.* (2021).[14] Briefly, HPC (molecular weight, M_W = 10 000 from Merck GB) and PAA (M_W = 3000 from Merck GB) were homogeneously blended in water with controlled pH values. Typically, 0.3, 0.5 and 0.7 mL of PAA were mixed with 0.5 g of HPC in 100 mL of deionized water under stirring at room temperature, respectively. Solution pH values were then adjusted using either 1.0 mol L^{-1} HCl (Fisher Scientific, UK) or 1.0 mol L^{-1} NaOH (Fisher Scientific, UK) stock solutions. Finally, bubbles were removed by centrifugation at 8000 rpm for 10 min to produce apparent hybrid HPC/PAA hydrogels.

Material characterization

The absorption and transmittance spectra of the hydrogel-filled glazing prototypes were measured on a LAMBDA 1050 UV/Vis/NIR spectrophotometer, PerkinElmer, from 200 to 2000 nm. A thermocouple was used to supply heat for lower and higher temperature-dependent spectrophotometry measurements. The effect of the temperature is solely considered for hydrogel solution only. The microstructural analysis of various temperature-treated hydrogel samples was executed using a scanning electron microscope (SEM) of FEI Quanta FEG 650. The Raman spectrum and mapping of the hydrogel were recorded using a WITec Alpha 300R. Attenuated total reflectance (ATR)-Fourier transform infrared (FTIR) spectroscopy of the hydrogel droplets was performed using a Bruker Alpha Platinum instrument. The temperature profile of the hydrogel-filled prototype chamber was measured under 1000 W m^{-2} (1 sun 1.5 AM) of light from a Wacom AAA+ continuous solar simulator (model WXS-210S-20).[3,24] The solar irradiances also varied between 900 W m^{-2} and 800 W m^{-2}, corresponding to 0.9 and 0.8 sun conditions. The indoor and outdoor incessant temperature recording was performed with a TC-08 thermocouple data logger (Pico Technology). The IR images were taken with an FLIR T425 camera positioned at a distance of 10 mm and then processed using corresponding software to develop the final images. A rapid freeze-drying technique with liquid nitrogen was conducted to keep the original microtexture for every thermal cycle.[25] The dynamic light scattering (DLS) measurements were performed using the Horiba Nano Partica – SZ 100 series.

Two significant transmission properties of glazing called luminous transmission or reflection (T_{lum}) and solar transmission (T_{sol}) were acquired from eqn (1) and (2),[3,24]

$$T_{lum} = \frac{\sum_{\lambda=380\ nm}^{780\ nm} y(\lambda)T(\lambda)\Delta\lambda}{\sum_{\lambda=380\ nm}^{780\ nm} y(\lambda)\Delta\lambda} \quad (1)$$

$$T_{sol} = \frac{\sum_{\lambda=200\ nm}^{2000\ nm} AM1.5(\lambda)T(\lambda,\alpha)\Delta\lambda}{\sum_{\lambda=200\ nm}^{2000\ nm} AM1.5(\lambda)\Delta\lambda} \quad (2)$$

where $T(\lambda)$ is the visible light spectral transmittance of the hydrogel filled glazing at a wavelength (λ), where 380 nm ≤ λ ≤ 780 nm, corresponding to human vision limits according to the CIE (International Commission on Illumination) standards.

The solar irradiance spectrum for an air mass of 1.5 (AM1.5 (λ)) was considered as the weighting function for the wavelength-dependent spectral transmittance. Besides, measurements corresponding to 510 nm represent the CIE photopic luminous human eye efficiency.[24] It should be noted that the transmission spectra results presented in this study are averaged values of ten repeated experiments. The high and low temperatures referred in this work are relative to the room temperature (22 °C) and relative humidity (~70%). In this work, the applied high and low temperatures were considered as the temperature usually corresponds to hotter and colder climates.

Fabrication of hybrid HPC/PAA hydrogel smart windows

Two 5 cm × 5 cm glass panes with a thickness of 1 mm were glued with an optimized gap of 0.5 mm at three edges with an opening on one side to infiltrate the hydrogel. Besides, the inter-glass pane gap was also varied between 0.2 mm and 1 mm to understand the effect of the gap between two glass panes on thermal comfort performance. The glass panes were further glazed using acrylonitrile butadiene styrene (ABS) polymer using the three-dimensional (3D) printing technique (ABS-P430 XL model, Stratasys, uPrint SE plus). Then, the HPC–PAA hydrogels were injected between two glass panes to get a prototype window. For temperature profile measurements, the prototype was covered with a 5 cm thick insulation material (Celotex GA4000). This is to confirm that the temperature gradient of the double-glazed prototype window can only be responsible for the incoming and outgoing lights passing through the glass panes and minimizing any other thermal effect. A data logger was fixed at the centre of the glass panes, which continuously monitored the indoor and outdoor temperatures with thermocouples for their temperature profile measurements. Photographs of the fabricated prototype and temperature profile measurement setup are presented in Fig. 1a and b, respectively. The amount of hydrogel infiltrated between two glass panes was dependent on their internal gap. 0.2 mL of hydrogel was sufficient for a 0.5 mm gap. For the 0.2 mm and 1 mm gap, the hydrogel amount was 75 μL and 0.48 mL, respectively.

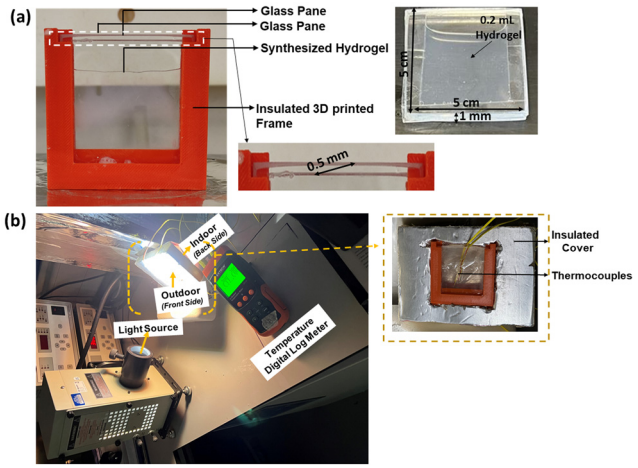

Fig. 1 Photographs along with a detailed view of the various components of the (a) fabricated hydrogel-filled double glazing window prototype, and (b) corresponding temperature profile measurement experiment setup as a function of time.

Results and discussion

Thermochromic behaviour of the HPC–PAA hydrogel

The hydrogel-filled window at pH 5.5 was treated at different temperatures to understand its thermochromism and cool/warm tone switchability. The hydrogel exhibits ~80% NIR light shielding (>1400 nm) at room temperature with ~90% visible transmittance (T_{vis}), as depicted in Fig. 2. Interestingly, there is a significant loss of visible transmittance during temperature modulation. At 40 °C, the T_{vis} was found to be ≤60%, whereas T_{vis} was reduced to ≤40% once the temperature was reduced to 5 °C. Noticeably, the NIR shielding maintained ≤40% irrespective of its applied temperature. It is anticipated that at a higher temperature, the PAA component exhibits stronger intramolecular interactions, leading to scattering centers that induce the scattering of the incident light aggregated polymer microparticles, whereas at a lower temperature, the aggregation could be dominated by HPC intermolecular hydrogen bonds that become dominant and could prevail between the polymer chains and surrounding water molecules.[26]

Effect of pH and water on the hydrogel's LCST and thermochromic properties

The HPC–PAA hydrogel matrix is formed by hydrogen bonds from the –OH groups in HPC and the –COOH groups in PAA chains, which is controlled by the solution pH.[23] As a result, the effect of solution pH can be a pivotal factor for hydrogel-based windows that also control the light transmission behaviour. Therefore, the pH variation of the prepared hydrogel was studied, which shows a consequential effect on the light transmittance property at room temperature. The hydrogel pH was adjusted with an aqueous solution of 1M HCl and NaOH. Fig. 3a describes the hydrogel-filled windows' transmittance spectra by varying the solution pH from 3.5 to 9.5. Stimulatingly, the nature of the hydrogel's transmittance spectra revealed unsubstantial changes

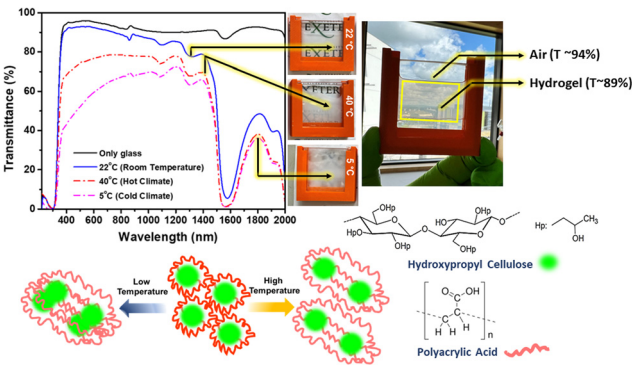

Fig. 2 Transmission spectra of HPC–PAA hydrogel-filled windows at different temperatures, along with their real-time photographs and schematic diagram offering reversible thermochromic phase transition, where T stands for transmittance.

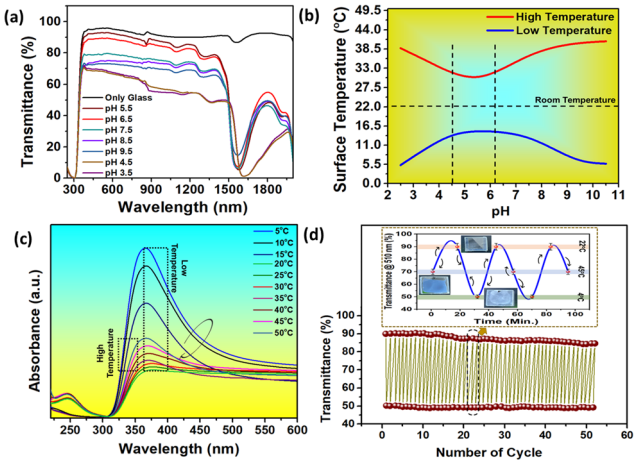

Fig. 3 (a) Transmittance spectra of the HPC–PAA hydrogel at different pHs, (b) corresponding surface temperature analysis when the incident temperature was set to 0 °C as lower and 50 °C as higher temperatures, respectively, (c) temperature-dependent absorption spectra of the HPC–PAA hydrogel at a pH of 5.5, and (d) thermo-kinetic cycle analysis at 510 nm of a hydrogel window.

across a wide range of pH. At lower pH's, there is a major T_{vis} reduction at 600–1400 nm, which is observed up to ~50%, while the T_{vis} reaches ~80% at pH 7.5. The resultant T_{vis} was found to be 3.5–4.5 < 5.5 > 6.5 > 7.5 > 8.5 > 9.5. Also, a relatively broad bathochromic shift was observed for the 1500–2000 nm zone at lower pHs when compared to other pHs. This might be due to the effect of polymeric agglomeration of HPC, which further separates PAA from its matrix and allows for comparably higher LCST.

Further, the temperature of the hydrogel was monitored under different pH conditions while increasing the incident temperature. The incident temperature is set to 5 °C (considering a lower temperature zone), which offers the maximum solution temperature range of ~11.8 to 15.2 °C for a pH range of 4–7. Fig. 3b exhibits the hydrogel LCST characteristics for higher and lower temperatures under different pH conditions. At a higher temperature, which was set to 50 °C, the minimum hydrogel temperature was found to be ~28–33 °C for a pH range of 4–7. The highest and lowest temperature was secured for pH 5.5 at colder and warmer climates, respectively and hence it was selected for further characterization.

At pH 5.5, the temperature-dependent absorption spectra of the hydrogel were recorded, where a relatively faster hypochromic shift was noticed at 320–450 nm while increasing the temperature from 5 °C to 25 °C. After 25 °C, a slight hyperchromic shift was spotted while increasing the temperature to 50 °C. A comparative result of faster and slower light absorption capacity while varying the temperature is shown in Fig. 3c. This result also corroborates with Fig. 2, where the hydrogels become semi-transparent at a lower temperature due to high light absorption.

Fig. 3d exhibits a highly repeatable cycle plot of the thermochromic hydrogel. The comprehensive testing was performed for up to 50 cycles. Besides, Fig. 3d shows the thermo-kinetic cycle analysis as a function of time at 510 nm according to a hydrogel-filled window's CIE photopic luminous human eye efficiency. The hydrogel started with a higher temperature (~40 °C), resulting in ~68% translucent characteristics. While dropping the temperature at a constant rate of 1 °C min^{-1} it reaches room temperature after 20 min, followed by a highly transparent characteristic of the same hydrogel. Further, decreasing the applying temperature successively reduced the transmittance to 50% and again, the transmittance enhanced to 90% once the temperature increased from 5 to 25 °C. This is a sinusoidal behaviour of the hydrogel's T_{vis} characteristics according to time recorded up to 100 min.

The LCST of the hydrogel is also dependent on its pH. Fig. 4a reveals that an optimum LCST was found between 35 and 35 °C for the HPC–PAA hydrogel in a pH range of 4.5–5.5. The LCST value is recommended for windows near room temperature with moderate pH. Therefore, considering both the parameters like pH and temperature contribution, the optimum LCST value at 35.2 °C found for pH 5.5 was selected. Under neutral and alkaline conditions, the formation of hydrogen bonds is limited due to the low activity of H^+, resulting in high LCST of the hydrogels similar to that of pure HPC.[27]

In contrast, the hydrogel exhibits translucent characteristics at higher temperatures, while at room temperature, it shows maximum light transmittance and minimum absorption. Frequently, water molecules remain within the hydrogels below the LCST, resulting in higher transparency and allowing the high solar transmission to heat the room in winter. The water molecules will be released from the hydrogel matrix, which forms polymeric shrinkage into the light scattering centres. Through pH reduction, emanate suppressed the deprotonation of the –COOH groups of PAA in the hydrogel, while solution pH surpasses the mutual hydrogen-bonding force between the –OH

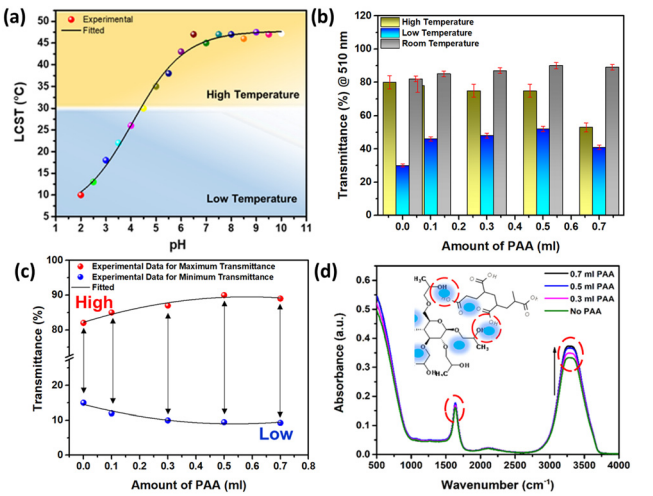

Fig. 4 (a) Effect of pH values on the LCST of the HPC–PAA hybrid hydrogels (the line between hot and cold temperatures represents the ideal LCST at 30 °C), effect of PAA amount for HPC–PAA hybrid hydrogels as a function of visible transmittance recorded at 510 nm for (b) hot, cold and room temperatures, (c) corresponding maximum and minimum temperature difference trend, and (d) ATR spectra of different PAA amounts compared within the absence of PAA for HPC–PAA hybrid hydrogels.

groups in HPC and the –COOH groups in PAA chains with the water molecules, which could reduce the LCST of the hydrogel.[28,29] A combined effect of hydrogel bonding, solution pH, and the mode of water molecule interaction on the hydrogel network becomes a deciding factor of the solution light transmittance character.[30,31]

The amount of PAA in the hydrogel formation was also evaluated under colder, room, and warmer temperatures. The presence of PAA in the hydrogel exhibits a steady increase and decrease trend of T_{vis} as a function of its concentration increase for hot and cold temperatures compared to the room temperature (Fig. 4b). The maximum difference of T_{vis} was observed for 0.5 mL of PAA addition, whereas above that, the corresponding T_{vis} becomes saturated, as shown in Fig. 4c. This may be due to the strength of hydrogen bonds that is maximum when the amount reached 0.5 mL, which is also noticed during the ATR analysis concerning the dedicated hydrogen bond peaks at 1520 and 3200 cm^{-1}, as shown in Fig. 4d. Similarly, a reversal in osmotic pressure difference can be placed during the temperature increase, resulting in the hydrogel network shrinkage and translucent behaviour. In contrast, a temperature decrease allows water to enter the hydrogel network, increasing the hydrogel's osmotic pressure, thus resulting in semi-transparency.

SEM and Raman characteristics of the thermochromic HPC–PAA hydrogel

Fig. 5(a)–(f) represents the SEM microstructural images at different magnifications. Increasing the temperature resulted in a relatively denser configuration of the HPC–PAA matrix than its as-prepared form. Interestingly, the pore diameters were also altered according to the temperature, which could be crucial in controlling the incoming light and heat.

Both the temperature and pH showed a linear relationship with the intermolecular gap of the hydrogels, as shown in Fig. 6a. Within the pH 4.5–6.2 and the temperature between 20 and 30 °C, the intermolecular gap exhibits a quite similar diameter range from 0.9 to 1.3 μm. This may be due to the incident temperature enhancement that facilitates the labile water egress that resulted in HPC agglomeration, resembling the increasing intermolecular gap value followed by a translucent behaviour to light, whereas at a lower temperature, more water molecules can enter the HPC–PLA matrix, affect the –C–O–C environment of the matrix network and hence show semi-transparency. This means that the temperature is the driving force influencing their interaction mode with the HPC–PAA matrix, followed by their light transmission behaviour. Besides the temperature, altering the pH of the hydrogel solution also proclaims similar characteristics. This is because of the supply of more OH– at higher pH and more H^+ at lower pH that can orient the hydrogel matrix's hydrogen bonding and electrostatic interaction.[27,30] Besides, the porosity modulation of hydrogel networking provides thermal insulation due to its thermal conductivity decreasing as its porosity increases due to an increasing amount of inside small-sized air pores.[31] An isotropic response was noticed due to randomly oriented hydrogels in the matrix.

To further study the water molecule contribution to temperature, Raman analysis was performed (Fig. 6b). The peaks at 3448 and 1721 cm^{-1} corresponded to the –OH group of the dominated water molecule; however, these values differ compared to their signature peak, which may be due to the oriented interaction with the HPC–PAA matrix. A distinct change was observed at 2879, 2941, and 2990 cm^{-1} peaks, primarily attributed to C–H stretching vibrations of the HPC network.[32] Also, the peaks at 848 cm^{-1}, which originated due to the H–C–H and H–C–O bending mode, and in the 1100–1300 cm^{-1} zone represent the H–C–H and C–OH–H twisting and rocking modes, and peaks from 1300 to 1730 cm^{-1} indicate the bending modes of C–O–H, H–C–H, and H–H–C bonds distributed in the HPC network, respectively.[33] Noticeably, all the signature Raman bands exhibited a bathochromic shift compared to their original states that strongly corresponds to moisture interaction induced by the temperature. Besides, at 4 °C, all the lower wavelength Raman peaks were relevantly less intense, followed by the absence of the C–H stretching peak in the 2800–3000 cm^{-1} zone and enhanced –OH stretching mode further signifies the possible way of water ingression inside the C–O–C network of the HPC matrix that resulted in semi-transparent behaviour to light.[34,35] However, at 45 °C, the –OH stretching mode was depressed by ~50%, followed by a significant increase of the C–H stretching peak to ~80%, indicating labile –OH hydrogen bond breaking and allowing for HPC aggregation, as shown in Fig. 5c and f, and hence resulting in translucent behaviour.

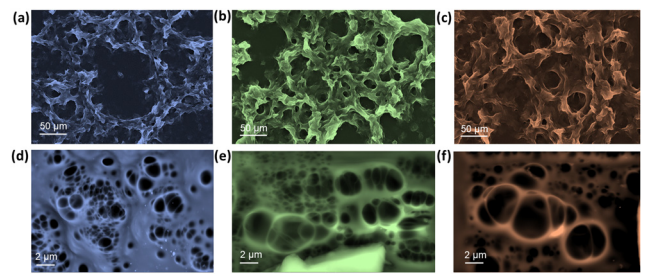

Fig. 5 SEM microstructure images of the HPC–PAA hydrogel at (a)–(d) 4 °C, (b)–(e) 22 °C, and (c)–(f) 45 °C for different magnifications, respectively.

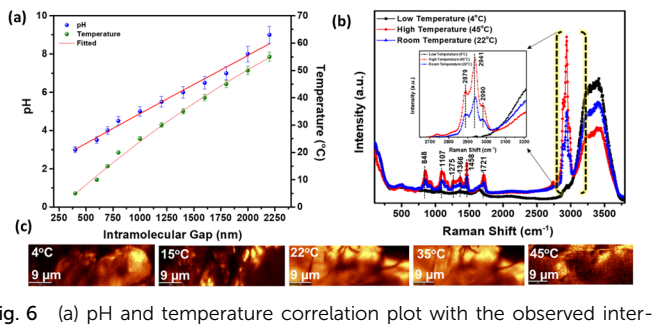

Fig. 6 (a) pH and temperature correlation plot with the observed intermolecular gaps resulting from the SEM analysis, (b) Raman spectra, and (c) corresponding images of the HPC–PAA hydrogel at different temperatures from 4 to 45 °C.

On the other hand, at room temperature (22 °C), the optimum hydrogen bonding and median Raman signal resulted in almost transparency. Fig. 6c represents temperature-dependent Raman images of the hydrogel sample taken during the measurement. It is evident from the Raman images that by increasing the temperature, the hydrogel network swaps its visual impression from denser to transparent to semi-transparency due to its intermolecular gap orientation, which corroborates with the SEM analysis.

Through the SEM and Raman spectra and image analysis, it is predicted that temperature influences the hydrogel network's intermolecular gap, which controls the transparency behaviour where water molecules play a pivotal role through their interaction with the HPC network. Sometimes, the polymer shrinkage results in Mie scattering.[36] A schematic representation of the overall plausible discussion is shown in Fig. 7. During DLS analysis, a significant change in the hydrodynamic diameter of the hydrogel was observed, which resulted in a disproportionate relation with the temperature. At room temperature, the hydrodynamic diameter of the hydrogel was ~600 nm. The hydrodynamic diameter was drastically changed to ~1.5 μm and ~350 nm from lower to higher temperature on the hydrogel. This may be an indirect observation where it is anticipated that at a higher temperature, the aggregation was dominated by PAA. At a lower temperature, the aggregation could be dominated by HPC, resulting in their osmotic pressure alteration and, thus, hydrodynamic size.[37]

Temperature regulation study of the hydrogel windows

The temperature regulation performance of the HPC–PAA hydrogel-filled windows was further analyzed by a prototype window constraining the sandwich-structured glazing system.

On illumination under 1 sun, the indoor temperature of the hydrogel-filled window was monitored and compared with that of the window without hydrogel filling (*i.e.*, air gap). Hydrogel filling exhibits a moderately lower temperature, on average ~28 °C. In contrast, the window without hydrogel filling resulted in a successive temperature increment to ~42 °C as measured up to 35 min of exposure, as shown in Fig. 8a. Similarly, at lower temperatures, the hydrogel-filled windows maintained the temperature on average at 15 °C, while the window without hydrogel filling exhibits a more substantial temperature reduction to 0 °C, as shown in Fig. 8b. The transmittance behaviour with and without the light condition can be visualized for the hydrogel filled window, as shown in Fig. S1 (ESI†), where a video of the transmittance of the hydrogel was recorded during light on and off conditions.

The temperature profile recorded for hydrogel-filled windows at higher and lower temperatures signifies excellent thermal comfort for all seasons. Besides, the temperature profile of the hydrogel-filled window was monitored under different solar irradiances, as shown in Fig. 8c. The varying incident solar irradiance such as 1 sun, 0.9 sun and 0.8 sun, further reflect the impact of PAA on the hydrogel formation. Uniform and steady heat release characteristics were also studied when the incident light was switched off, enabling the heat preservation characteristic. However, the temperature reduction rate further accelerates once PAA is incorporated, directly controlling the LCST of the HPC–PAA hydrogel matrix. Fig. 8d exhibits the IR thermal processed images captured at different times on their outdoor and indoor surfaces while increasing the temperature from 20 °C to 50 °C. The outdoor temperature increases during the 1 sun illumination to 50 °C, while the corresponding indoor temperature remains at 25–30 °C simultaneously. Transmittance and temperature regulating hydrogel-filled windows exhibit a minimum trade-off between them, making the windows a smart solution for energy-saving in the built environment.[38,39]

The maximum temperature difference was also recorded as a function of time, as shown in Fig. 9a, where the average temperature difference showed an almost similar trend of ~12 °C as recorded up to 35 min compared to the maximum outdoor temperature. The gap between the two glass panes was

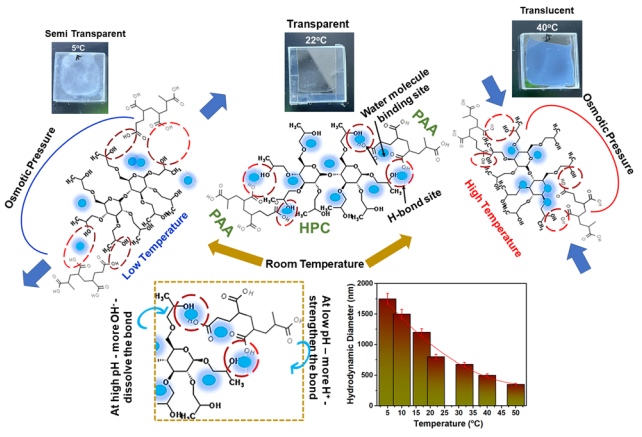

Fig. 7 Schematic representation of the possible temperature-pH-transparency tuning mechanism of the HPC–PAA hydrogel for optimal climate-adaptable energy saving smart windows along with temperature-dependent DLS measurements.

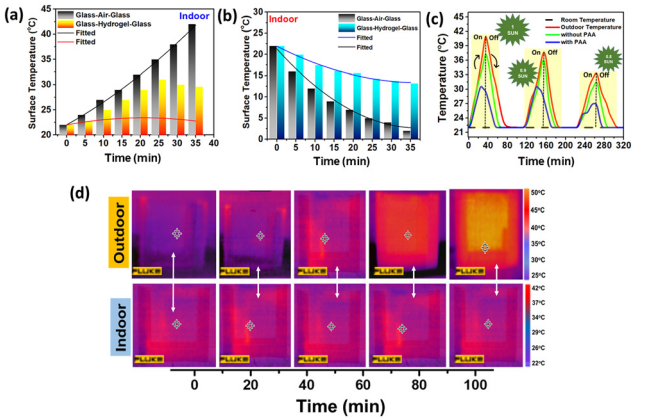

Fig. 8 The indoor temperature profile of the HPC–PAA hydrogel-filled window for (a) warmer and (b) colder climates, compared with the air-filled window as a function of time, and (c) under various solar irradiances as a function of time and PAA role, respectively, and (d) IR thermal images of indoor and outdoor glass panes of the HPC–PAA hydrogel filled window recorded at the same time.

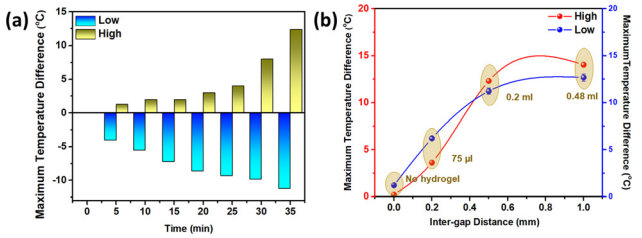

Fig. 9 The maximum temperature difference between indoor and outdoor temperatures is recorded (a) as a function of time when the inter-gap distance was 0.2 mm, and (b) as a function of inter-gap distance for different hydrogel amounts mentioned in golden colour.

also varied, which controlled the temperature gradient of the glazing. Fig. 9b exhibits the recorded maximum temperature during the temperature tuning for different inter-gap distances, establishing a proportional relationship between the temperature difference and inter-gap distance. However, a negligible temperature difference is observed in the absence of the hydrogel (only air). The optimum inter-gap distance was 0.5 mm, resulting in a rapid and improved temperature difference, especially for higher temperature conditions.

Further increment of inter-gap distance certainly enhances the temperature difference, while the rate of temperature enhancement was quite similar and may reach a saturation point. Besides, higher inter-gap distances indicate higher hydrogel infiltration which is expected to provide better thermal comfort. Therefore, an optimum balance between inter-gap distance, temperature difference and hydrogel amount was secured by 0.5 mm inter-gap distance, supported by Fig. 9a. Notably, these results manifest an understanding of simultaneously maximizing temperature differences that ensures a smart window for both temperature differences and a smart, intelligent window for cold and warm climates.

Fig. 10a reveals the hydrogel-filled window's visible luminous transmittance (T_{lum}) and solar modulation ability (T_{sol}) for various solution pH. The T_{lum} and T_{sol} values follow a steady enhancement when the pH increases from 3.5 to 5.5, and both values become saturated further. The highest T_{lum} and T_{sol} values were found at 90.1% and 82.7%, respectively, for pH 5.5, which supports that pH 5.5 was the optimum, which exhibits a minimum trade-off between temperature and transmittance of the hydrogel. Fig. 10b represents the optical properties observed

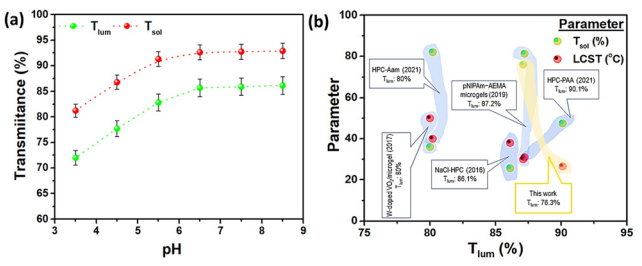

Fig. 10 (a) pH-dependent luminous and solar transmission plot of the HPC–PAA hydrogel filled window, and (b) comparison of the luminous transmission, solar transmission, and LCST parameters with the current work.[14,19,40–42]

in recently reported hydrogel-filled glazing in comparison with this work. Maintaining a high T_{lum} and T_{sol} with a lower LCST is the novelty of this work, where most of the other hydrogels are struggling to maintain these parameters.

Conventional energy-saving windows do not regulate visible light, which can engender building heating. Considering factors like fabrication-installation cost, carbon footprint, and energy security, the properties of hydrogels make them an emerging option to be engineered to meet the desired requirements. Hydrogel-filled windows are considered the functional component for constructing smart windows due to their high transparency and suitable LCST. Hydrogels are cost-effective, combined with temperature response and pH response simultaneously. Due to containing water, hydrogels allow an extensive amount of thermal energy to be stored instead of getting transferred through the glass during the daytime.

In contrast, the heat can be then gradually cooled and released at night, simultaneously enabling thermal comfort and energy conservation. The development of such an advanced glazing technology has the potential to achieve energy-positive buildings by substantial annual energy reduction.[43] Also, the near IR shielding can be more substantial while incorporating the local surface plasmon resonance transition materials like WO_3. Nevertheless, revamping energy-saving smart windows, thermochromic hydrogels' unique tunable scattering behaviours can also be applied to optical modulators and various displays. This study on hydrogel glazing systems should be extended to determine the most energy-efficient retrofit design by applying large-scale experiments or a mathematical model.

Conclusions

In conclusion, the HPC–PAA hydrogel exhibits a lower LCST range from 20 to 35 °C across the pH of 4.5–6.3. Further, the hydrogel-filled window provides a comfortable indoor living environment even in hot and cold climates. The hydrogel was responsive to moderate transparency (on average ~70%) from 400 to 1400 nm in a wide temperature range (5–40 °C), while the transparency was relatively lowered to <50% at >1400 nm. Also, the hydrogel transparency was significantly dropped to <5% at <400 nm. The hydrogel exhibited a high luminous transmittance (T_{lum} = 90.1%) and excellent solar energy modulation (T_{sol} = 80%) for pH 5.5 with a periodic semi-transparent to translucent *via* transparent cycle, relevant for developing advanced glazing. Including water molecules, followed by incident temperature treatment, controls the transmittance characteristics of the hydrogel. Hydrogel glazing potentially acts as a glare-free daylight option that can control the heat loss and heat gain according to the outdoor climate of the house. In addition, electrochromic–thermochromic regulated active control could be combined with the hydrogels for better light modulation and energy utilization. Cost-effective hydrogels can be integrated as a potential pathway to extend the facile laboratory-based process to large-scale, cost-effective industrial volume production as a suitable replacement for expensive vacuum glazing systems.

Author contributions

AR performed the experiments, comprehensive study and manuscript drafting. TKM and AAT provided their guidance, co-designed and supervised the work. AAT is the project leader of this work.

Conflicts of interest

There are no conflicts to declare.

Acknowledgements

This work was funded by the Engineering and Physical Sciences Research Council (EPSRC), UK, under research grant numbers EP/T025875/1 and EP/V049046/1. However, EPSRC was not directly involved in the writing of this article. The authors acknowledge the help rendered for the ATR characterization by Prof. Francesca Palombo, Associate Professor of Biomedical Spectroscopy, University of Exeter, Streatham Campus, UK. The authors would also like to acknowledge Dr Ellen Green, Unit of Activity Manager Biophysics, College of Engineering, Mathematics and Physical Sciences, University of Exeter, Streatham Campus, UK, for her assistance in the Raman spectroscopy characterization. The authors are also thankful to Dr Yusuf Chanchangi, Postdoctoral Researcher, University of Exeter, Penryn Campus, UK, for his help in 3D printing.

References

1 Y. Zhou, X. Dong, Y. Mi, F. Fan, Q. Xu, H. Zhao, S. Wang and Y. Long, *J. Mater. Chem. A*, 2020, **8**, 10007–10025.
2 G. Xu, H. Xia, P. Chen, W. She, H. Zhang, J. Ma, Q. Ruan, W. Zhang and Z. Sun, *Adv. Funct. Mater.*, 2022, **32**(5), 2109597.
3 A. Roy, H. Ullah, A. Ghosh, T. K. Mallick and A. A. Tahir, *Constr. Build. Mater.*, 2022, **331**, 127319.
4 M. Yu, Y. Shi, R. Li and P. Wang, *ACS Appl. Mater. Interfaces*, 2018, **10**(46), 39819–39827.
5 E. L. Runnerstrom, A. Llordés, S. D. Lounisa and D. J. Milliron, *Chem. Commun.*, 2014, **50**, 10555–10572.
6 N. Youngblood, C. Talagrand, B. F. Porter, C. G. Galante, S. Kneepkens, G. Triggs, S. G. Sarwat, D. Yarmolich, R. S. Bonilla, P. Hosseini, R. A. Taylor and H. Bhaskaran, *ACS Photonics*, 2022, **9**(1), 90–100.
7 Y. Guo, J. Bae, Z. Fang, P. Li, F. Zhao and G. Yu, *Chem. Rev.*, 2020, **120**(15), 7642–7707.
8 X. Wang and S. Narayan, *Front. Energy Res.*, 2021, **9**, 800382.
9 J. Zhang, C. Wang, F. Liu and C. Dong, *J. Therm. Anal. Calorim.*, 2022, **147**, 7729–7740.
10 C. Lin, J. Hur, C. Y. H. Chao, G. Liu, S. Yao, W. Li and B. Huan, *Sci. Adv.*, 2022, **8**, eabn7359.
11 Y. Zhou, Y. Cai, X. Hu and Y. Long, *J. Mater. Chem. A*, 2014, **2**, 13550–13555.
12 H. Seddiqi, E. Oliaei, H. Honarkar, J. Jin, L. C. Geonzon, R. G. Bacabac and J. Klein-Nulend, *Cellulose*, 2021, **28**, 1893–1931.
13 D. Cao, C. Zhu, W. Lu, C. Qin and S. Cheng, *Sol. RRL*, 2018, **2**(4), 1700219.
14 L. Zhang, H. Xia, F. Xia, Y. Du, Y. Wu and Y. Gao, *ACS Appl. Energy Mater.*, 2021, **4**(9), 9783–9791.
15 Y. Zhou, S. Wang, J. Peng, Y. Tan, C. Li, F. Y. C. Boey and Y. Long, *Joule*, 2020, **4**(11), 2458–2474.
16 M. Stuart, W. T. S. Huck, J. Genzer, M. Müller, C. Ober, M. Stamm, G. B. Sukhorukov and I. Szleifer, *et al.*, *Nat. Mater.*, 2010, **9**, 101–113.
17 P. Heidarian, A. Kaynak, M. Paulino, A. Zolfagharian, R. J. Varley and A. Z. Kouzani, *Carbohydr. Polym.*, 2021, **270**, 118357.
18 G. Sennakesavan, M. Mostakhdemin, L. K. Dkhar, A. Seyfoddin and S. J. Fatihhi, *Polym. Degrad. Stab.*, 2020, **180**, 109308.
19 Y. S. Yang, Y. Zhou, F. B. Y. Chiang and Y. Long, *RSC Adv.*, 2016, **6**, 61449–61453.
20 F. F. Xin, Q. L. Lu, B. X. Liu, S. C. Yuan, R. L. Zhang and Y. Wu, *Eur. Polym. J.*, 2018, **99**, 65–71.
21 Y.-Q. Feng, M.-L. Lv, M. Yang, W.-X. Ma, G. Zhang, Y.-Z. Yu, Y.-Q. Wu, H.-B. Li, D.-Z. Liu and Y.-S. Yang, *Molecules*, 2022, **27**, 1638.
22 X. H. Lu, Z. B. Hu and J. Schwartz, *Macromolecules*, 2002, **35**, 9164–9168.
23 R. S. Yao, J. J. Xu, X. H. Lu and S. S. Deng, *J. Nanomater.*, 2011, **2011**, 507542.
24 A. Roy, H. Ullah, M. Alzahrani, A. Ghosh, T. K. Mallick and A. A. Tahir, *ACS Sustainable Chem. Eng.*, 2022, **10**, 6609–6621.
25 A. Eklund, H. Zhang, H. Zeng, A. Priimagi and O. Ikkala, *Adv. Funct. Mater.*, 2020, **30**, 2000754.
26 M. Martin-Pastor and E. Stoyanov, *J. Polym. Sci.*, 2020, **58**(12), 1632–1641.
27 X. Zhang, F. Lin, Q. Yuan, L. Liu, C. Wang and S. Wang, *Carbohydr. Polym.*, 2019, **215**, 58–62.
28 A. Eklund, H. Zhang, H. Zeng, A. Priimagi and O. Ikkala, *Adv. Funct. Mater.*, 2020, **30**, 2000754.
29 R. Zhang, B. Xiang, Y. Shen, L. Zia, L. Xu, Q. Guan and S. Tang, *J. Mater. Chem. A*, 2021, **9**, 17481–17491.
30 C. Nakamura, T. Yamamoto, K. Manabe, T. Nakamura, Y. Einaga and S. Shiratori, *Ind. Eng. Chem. Res.*, 2019, **58**, 6424–6428.
31 S.-N. Hong, C.-J. Yu, U.-S. Hwang, C.-H. Kim and B.-H. Ri, *Mater. Chem. Phys.*, 2020, **250**, 123146.
32 J. Rohowsky, K. Heise, S. Fischer and K. Hettrich, *Carbohydr. Polym.*, 2016, **142**, 56–62.
33 F. Adar, *Spectroscopy*, 2016, **31**(11), 22–27.
34 U. P. Agarwal, *Molecules*, 2019, **24**(9), 1659.
35 Y. Guan, Y. J. Zhang, T. Zhou and S. Q. Zhou, *Soft Matter*, 2009, **5**, 842–849.
36 A. Nakamura, R. Ogai and K. Murakami, *Sol. Energy Mater. Sol. Cells*, 2021, **232**, 111348.
37 A. Bhattacharyya, C. O'Bryan, Y. Ni, C. D. Morley, C. R. Taylor and T. E. Angelini, *Biotribology*, 2020, **22**, 100125.
38 Y.-S. Yang, Y. Zhou, F. B. Y. Chiang and Y. Long, *RSC Adv.*, 2017, **7**, 7758–7762.

39 M. J. Serpe, *Nature*, 2019, **565**, 438–439.
40 X.-H. Li, C. Liu, S.-P. Feng and N. X. Fang, *Joule*, 2019, 3(1), 290–302.
41 W. Wu and H. H. Skye, *Renewable Sustainable Energy Rev.*, 2021, **142**, 110859.
42 L. Zhang, Y. Du, H. Xia, F. Xia, G. Yang and Y. Gao, *Ceram. Int.*, 2022, DOI: **10.1016/j.ceramint.2022.08.288**.
43 W. Wu and H. H. Skye, *Renewable Sustainable Energy Rev.*, 2021, **142**, 110859.